

Digital Low-Level RF control system for Advanced Light Source Storage Ring

Qiang Du*, Lawrence Doolittle, Michael Betz, Benjamin Flugstad, Massimiliano Vinco, and Kenneth Baptiste

Lawrence Berkeley National Laboratory
1 Cyclotron Rd, Berkeley, CA, 94720 USA

Abstract—We have commissioned the digital Low Level RF (LLRF) system for storage ring RF at Advanced Light Source at Lawrence Berkeley National Lab (LBNL). The system is composed of 42 synchronous sampling channels for feedback control, diagnostics, and interlocks. The closed loop RF amplitude and phase stability is measured as $< 0.1\%$ and $< 0.1^\circ$ respectively, and the real-time machine protection interlock latency is measured $< 2.5\mu\text{s}$. We have also developed PLC-FPGA-EPICS interfaces to support system configurations between hybrid operation modes using two klystrons driving two RF cavities at 500MHz resonance frequency. The deployed LLRF system has been operating since March 2017.

I. INTRODUCTION

The Advanced Light Source (ALS) at Lawrence Berkeley National Laboratory is a U.S. Department of Energy's synchrotron light source user facility that is operational since 1993. With circumference of 196.8 m, the ALS Storage Ring (SR) keeps electron beam current of 500 mA at 1.9 GeV under multi-bunch mode user operation to deliver synchrotron X-rays to surrounding 40 experimental end stations. As the electron beam loses energy every turn due to synchrotron radiation, two normal conducting RF cavities provides a total of ~ 1.3 MV acceleration voltage and keeps the beam energy constant against variable beam loads and many sources of instabilities.

The two cavities are driven by two 300 kW klystrons at 499.642 MHz through a waveguide matrix system, which can be configured to switch RF drive mode among different modes. As shown in Figure 1, 5 configurable RF drive modes includes each klystron driving one cavity, one klystron driving two cavities or test loads for RF test.

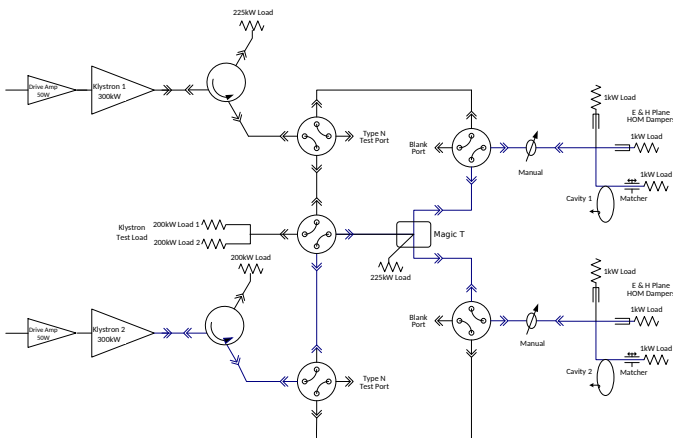


Fig. 1: Configurable waveguide mode to drive two cavities

Table I shows typical values of storage ring (SR) RF power requirement for nominal user operation for both ALS at 1.9 GeV 500 mA multi bunch mode, and the planned ALS-Upgrade (ALS-U) project at 2.0 GeV.

	ALS	ALS-U	
Number of Klystrons	2		
Number of Cavities	2		
Cavity Q_0	28670		
Cavity Q_L	16700		
Harmonic number h	328	327	
Circumference	196.8	195.94	m
Beam energy	1.9	2.0	GeV
Cavity RF Frequency	499.64	500.394	MHz
$\frac{R}{Q}$ (ea)	4.9	4.9	MΩ
Cavity voltage	671	300	kV
β	2.9	10.07	
Energy loss per turn	329	329	keV
BM Beam Power	141	125	kW
ID Beam Power	42	35	kW
3HC Beam Power	7.3	4.4	kW
Parasitic Beam Power	2.9 (est.)	2.2 (est.)	kW
Total Beam Power	192.9	166.9	kW
Cavity Power(no beam)	46	9.2	kW
Cavity Power(beam)	142.5	127.6	kW
Waveguide Loss	9.2 (est.)	2.6 (est.)	kW
High Power Amplifier	294.0	257.8	kW

TABLE I: ALS and ALS-U Storage Ring RF parameters

As part of the ALS RF system upgrade project, the digital LLRF system was designed to replace the analog controller [1] and corresponding RF interlock systems, with design parameters and requirements listed in Table II. The digital LLRF system was installed and commissioned in March 2017, and was operational since then. It is expected that the current LLRF design would still meet ALS-U SR RF specifications, except ALS-U would have additional LLRF control requirements to its accumulator ring RF.

	Analog LLRF	Digital LLRF	
Num. RF Drive Modes	1	5	
Num. RF Signals	4	42	
Amp. Loop Bandwidth	3.5	1	kHz
Phase Loop Bandwidth	3.6	1	kHz
Phase Jitter [10Hz,1MHz]	< 3	< 0.6	ps
Interlock latency	< 100	< 4	μs
Amp. stability	0.56	< 0.1	%
Phase stability	1.8	< 0.1	°

TABLE II: Analog LLRF performance and requirements to digital LLRF control

The digital LLRF consists of three connected FPGA chassis: LLRF chassis, RF monitor (RFMON) chassis and Fast Interlock chassis as shown in 2. The LLRF chassis generates a common LO reference from ALS master oscillator for synchronous digitizing and digital signal processing clocks for all 42 RF signals, and two processed IQ streams from LLRF and RFMON chassis are sent to Fast Interlock

chassis for centralized interlock processing together with 16 channels of ARC detectors.

Each FPGA chassis has Gigabit Ethernet communication to a local computer that hosts EPICS Input-Output-Controller(IOC) to access all raw and processed registers, and configurable waveforms. Fast Interlock chassis has a dedicated communication to master interlock PLC, so that all interlock settings are directly available from PLC, which holds the RF drive mode and waveguide matrix configuration information.

The PLC-FPGA interlock system is designed to be software-free, so that the operation reliability and interlock invulnerability would not be impacted by external components such as EPICS, network or any operating system issues.

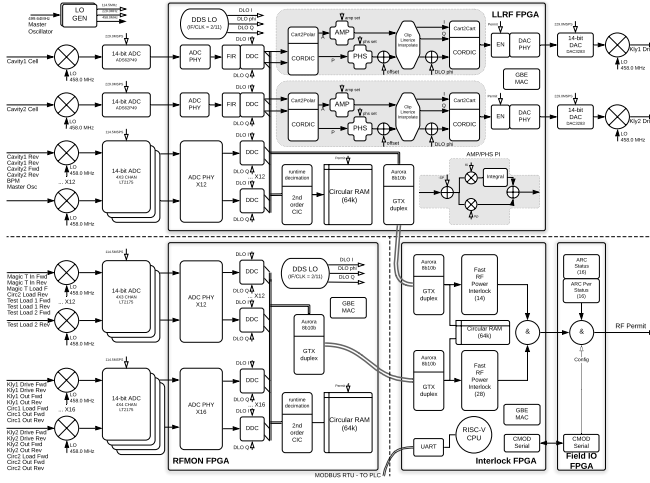


Fig. 2: ALS storage ring digital LLRF system overview

II. HARDWARE DESIGN

A. Frequency configuration

Both LO and sampling frequency are derived from ALS master oscillator f_{MO} .

$$\begin{aligned} f_{MO} &= 499.645 \text{ MHz} \\ f_{LO} &= \frac{11}{12} \cdot f_{MO} = 458.008 \text{ MHz} \\ f_{IF} &= \frac{1}{12} \cdot f_{MO} = 41.636 \text{ MHz} \\ f_{S1} &= \frac{1}{2} \cdot f_{LO} = 229.004 \text{ MHz} = f_{dsp} \\ f_{S2} &= \frac{1}{4} \cdot f_{LO} = 114.502 \text{ MHz} \end{aligned}$$

B. Low-Level RF chassis

The LLRF chassis uses Abaco Systems FMC150 and FMC112 with Xilinx KC705 FPGA carrier board for digital platform. FMC150 provides 2 14-bits ADC and 2 16-bits DAC channels at f_{S1} for precision control, and FMC112 provides 12 14-bits ADC at f_{S2} for RF monitoring. Two Gigabit transceivers (GTX) links are used for inter-FPGA communication via optic fiber (SFP+) for interlocking and timing distribution respectively.

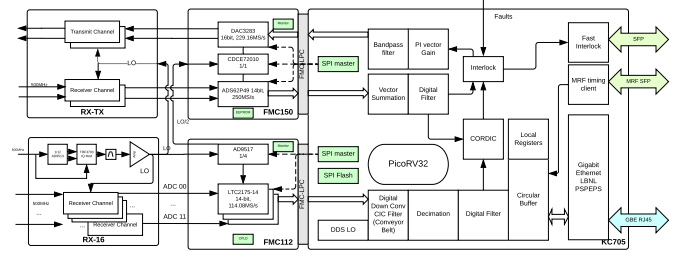
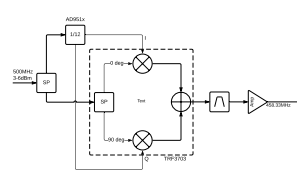
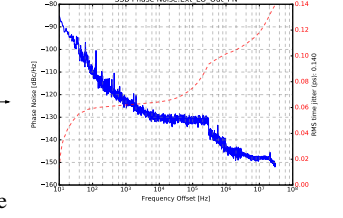


Fig. 3: LLRF chassis hardware configuration

1) *Single Side Band LO generation*: f_{LO} is generated using single side band modulation by a frequency divider AD9513 and a vector modulator TRF3703, as shown in Figure 4a. Because both chips are not sensitive to clock signal level, the generated LO level is stable against MO signal level variations. The carrier feed through and image frequency suppression is also benefited as shown in Table III. When using an external signal source with 107 fs rms phase jitter at f_{MO} , the measured phase noise of f_{LO} is 140 fs rms [1Hz, 20MHz].



(a) SSB LO generation scheme



(b) Phase Noise of Generated LO

Carrier feed-through	-45.4	dB
Image frequency suppression	-59.3	dB
LO phase jitter	140	fs (rms)
LO level variation over a week	< 0.005	dBm (p2p)

TABLE III: Measured performances of generated LO

2) *Analog RF Frontend*: All RF signals are down converted to f_{IF} for digitization using a home-built analog frontend boards. A 16 channel down converter is designed in order to interface FMC112/FMC116 as shown in Figure 5.

This frontend board features single side band LO generation and distribution, externally synchronizable switch DC power supply, individual linear regulator for each channel, high channel isolations, and environmental monitoring for voltage, current, LO level and temperature.

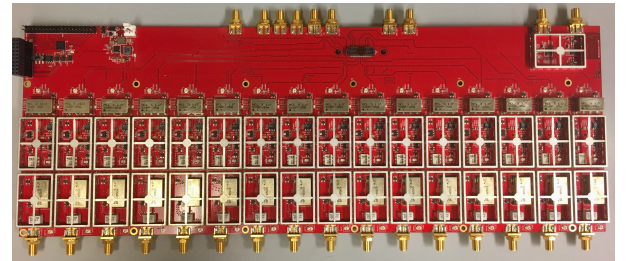


Fig. 5: Self-stackable 16 channels down-converter

The cross talk between channels is optimized by using RF shielding, various attenuation and filtering in LO path, and individual low noise

local voltage regulators. It is measured as better than 50 dB when using the high density connector for FMC112/FMC116.

3) *ADC benchmark:* By injecting a near full scale signal at f_{MO} , all ADC channels including analog down conversion are benchmarked to match data sheet specifications.

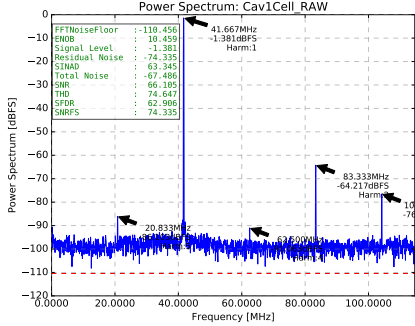
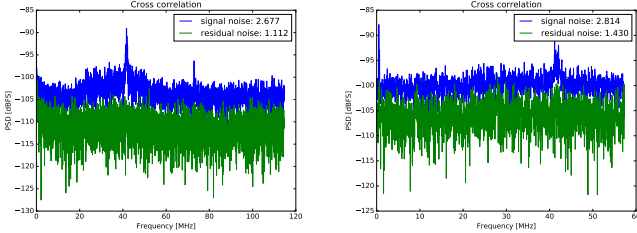


Fig. 6: FMC150 ADC1 spectrum

In order to separate signal against common components between ADC channels such as f_{MO} feedthrough, LO and common power supply noise, we used cross correlation between channel x and y to measure residual ADC noise [2].

$$P_{res} = \frac{1}{2} (\langle F_x \cdot F_x^* \rangle + \langle F_y \cdot F_y^* \rangle - 2\langle F_x \cdot F_y^* \rangle)$$

$$N_{res} = \sqrt{\sum_k P_{res}(k)}, \quad SNR_{res} = 20 \log \left(\frac{2^{13}}{\sqrt{2} \cdot N_{res}} \right)$$



(a) FMC150 residual noise

(b) FMC112 residual noise

	Specified	Measured	
Total SNR	71	66	dBFS
SNR _{res}	75	74.34	dBFS
Isolation (feedback)		> 72	dB
Isolation (interlock)	55	> 50	dB

TABLE IV: Measured ADC benchmarks

It is concluded that the analog frontend together with digitization platform meets the design specifications.

4) *DAC benchmark:* The phase noise of two DAC output signal at f_{MO} after up conversion are measured as < 130 fs (rms) [1Hz, 20MHz] using a signal source analyzer (Rohde & Schwarz FSUP) which also met design specification, as shown in Figure 8.

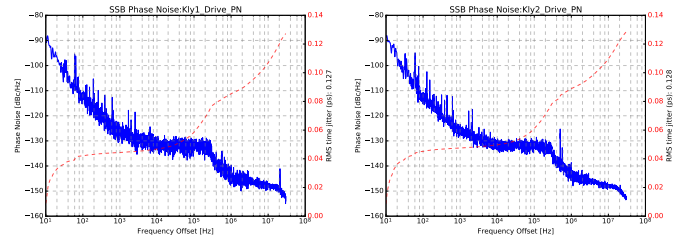


Fig. 8: DAC1 and DAC2 phase noise measurement

C. RF Monitor chassis

The RF monitor chassis uses Abaco Systems FMC112 and FMC116 with Xilinx KC705 FPGA carrier, as in Figure 9. Two 16-channel down conversion frontend boards are used to host 28 channels. LO signal are from LLRF chassis to keep the same frequency divider states for RF phase measurement. All sampling frequencies are at f_{S2} and FPGA clock is running at twice as fast as f_{S1} . The communication interfaces are common to LLRF chassis.

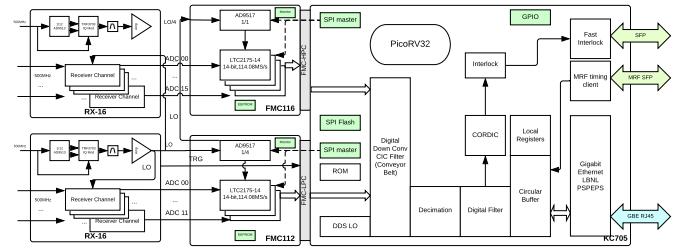


Fig. 9: RF Monitor chassis hardware configuration

D. Fast Interlock Chassis

Also based on Xilinx KC705, the Fast Interlock Chassis uses two GTX links to collect and process IQ streams from LLRF and RFMON chassis, with addition of 16 channels of arc detectors faults and arc power faults through a Field IO FPGA (Digilent CMOD S6). The standalone reference clock is tuned to be within ± 100 ppm of stream clock at f_{dsp} .

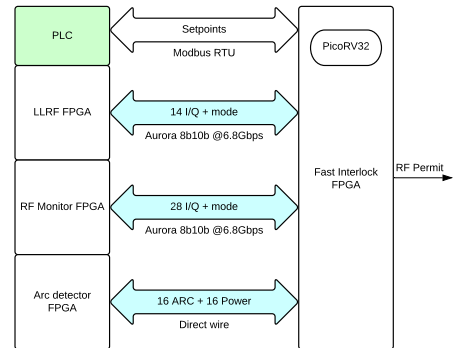


Fig. 10: Fast Interlock Chassis logic diagram

All interlock configurations and setpoints are passed by PLC–FPGA communication, and the end-to-end interlock latency needs to be < $4\mu s$.

III. FIRMWARE DESIGN

A. Digital Signal processing

1) *Direct Digital Down-conversion*: Non-IQ sampling avoids aliasing for high precision digitization.[3] In our case, with $\frac{f_{IF}}{f_{sample}} = \frac{2}{11} = \theta \simeq 65.45^\circ$, one can construct direct digital down-conversion (DDC) using two consecutive ADC samples y_n, y_{n+1} . The coefficient matrix is generated using a Coordinate Rotation Digital Computer (CORDIC).

$$\begin{pmatrix} y_n \\ y_{n+1} \end{pmatrix} = \begin{pmatrix} \cos(n\theta) & \sin(n\theta) \\ \cos((n+1)\theta) & \sin((n+1)\theta) \end{pmatrix} \begin{pmatrix} I \\ Q \end{pmatrix}$$

$$\begin{pmatrix} I \\ Q \end{pmatrix} = \frac{1}{\sin \theta} \begin{pmatrix} \sin((n+1)\theta) & -\sin(n\theta) \\ -\cos((n+1)\theta) & \cos(n\theta) \end{pmatrix} \begin{pmatrix} y_n \\ y_{n+1} \end{pmatrix}$$

2) *Double-time signal process*: Because $f_{dsp} = 2f_{s2}$, and also the need for dynamically configure feedback signal paths according to RF drive mode, it is desired to have two DSP clock cycles per ADC sample in order to reuse the same pipeline for different combinations of RF signal processing. Figure 11 shows an example of pipe lining two ADC channels to a stream of digitally down converted IQ pairs.

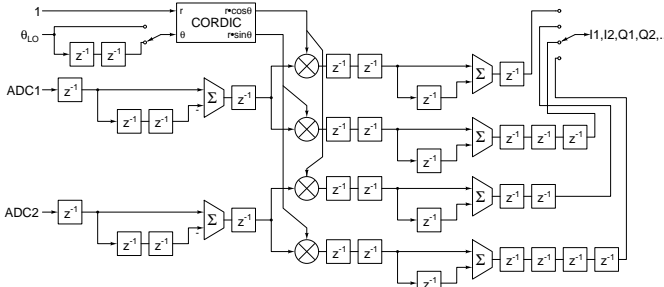


Fig. 11: double-time: Two DSP clock cycles per ADC sample

3) *Feedback controller*: The feedback controller is constructed as shown in Figure 12.

The framed IQ pairs, in our case two cavity probe signals are converted to amplitude and phase in order to compare with loop sepoints, and fed into a set of proportional-integral controllers with limiter. The clipped output is then digitally up converted using an output CORDIC with an optional phase shifter to compensate variable loop group delay. When RF permit signal is valid, the loop output signal is sent to each DAC.

There are amplitude and phase loops for each klystron. For one klystron driving two cavities of test loads, the weighted average of two cavity probe amplitudes are used for amplitude loop, and one cavity phase for phase loop.

$$C(z) = K_p + K_i \frac{1}{1 - z^{-1}}, \quad T = \frac{4}{f_{clk}}$$

Since the exact controller transfer function is known by design, the loop register scaling are verified using an IIR cavity emulator in z domain.

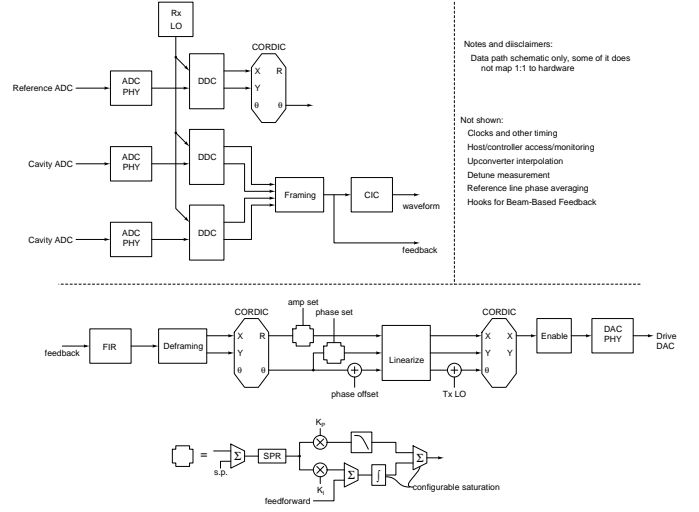


Fig. 12: LLRF firmware overview

4) *Waveform*: All baseband signal after DDC are serialized onto a conveyor belt signal stream to apply a run-time configurable CIC filter for different decimation factors.

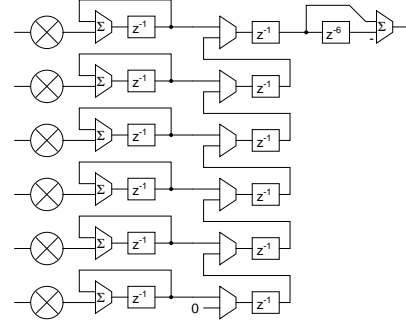
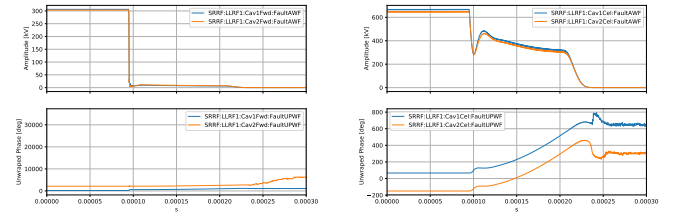


Fig. 13: signal pipe line with CIC filter

Features of waveform handling includes dynamic channel selection, collision-free doubled buffer structure, associated statistics with timestamps, and fault capturing.



(a) Cavity forward signals

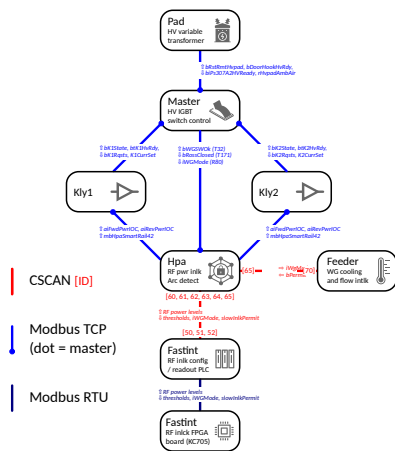
(b) Cavity probe signals

Fig. 14: Fault Waveform Capturing

Figure 14 shows an example of fault waveform capturing at an event of RF trip, when both cavities were only driven by beam after LLRF permit was removed. This is an essential feature for finding the root cause of RF system trip.

5) *Peripheral management*: There are hundreds of registers and complicated processes involved in initialization process to bring the system to nominal state from power up. An open source RISC-V

6) *PLC-FPGA interface:* PicoRV32 in Fast Interlock Chassis also handles direct interfacing with PLC via ModbusRTU. The multi-chassis FPGA system works as a peripheral from PLC point of view as shown in Figure 16.

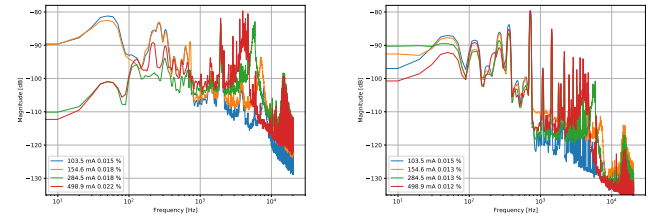


IV. SOFTWARE DESIGN

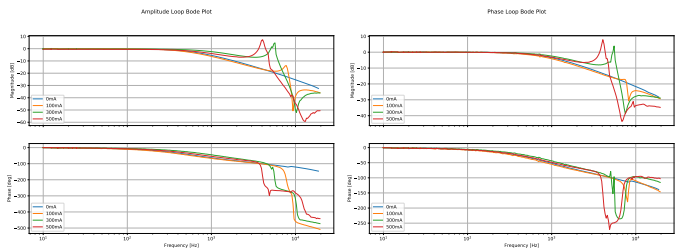
V. OPERATION AND PERFORMANCE

We have measured both amplitude and phase loop noise spectrum density from in-loop waveform data at different beam currents as shown in Figure 17. The data was measured under klystron 2 drive mode, where average of two cavity cell voltages are regulated. Loop parameters are at operation nominal setting, with ~ 1 kHz bandwidth, integral only. It is observed that, as beam current increased from 103 mA to 499 mA, the synchrotron frequency moved from < 10 kHz towards ~ 4 kHz, and its contribution became more significant. Within analyse bandwidth of [10Hz, 20kHz], the amplitude loop stability is measured as $< 0.03\%$ rms, and phase loop stability is $< 0.02^\circ$ rms.

By injecting a excitation tone on either amplitude or phase loop setpoint, the closed loop frequency response could be measured as



a function of excitation frequency. We have measured bode plots at different beam currents as shown in Figure 18. Both amplitude and phase loop unity gain is observed around 1 kHz, as expected. Again, beam induced synchrotron frequencies contributes as a resonance peak outside loop bandwidth.



C. Hard real-time RF interlock

RF Power (Lab)	1.45	μs
RF Power (ALS)	< 3	μs
ARC det. latency	< 2	μs

VI. CONCLUSION

ACKNOWLEDGMENT

This work is supported by the Office of Science, Office of Basic Energy Sciences, of the U.S. Department of Energy under Contract No. DE-AC02-05CH11231.

- [1] C. Lo, B. Taylor, and K. Baptiste, "The amplitude and phase control of the als storage ring rf system," in *Proceedings Particle Accelerator Conference*, vol. 2. IEEE, 1995, pp. 801–803.
- [2] L. Doolittle, G. Huang, K. Campbell, E. Cullerton, and J. Jones, "LCLS-II LLRF Loopback Test Results," 2016, <http://recycle.lbl.gov/~ldoolitt/loopback>.
- [3] L. Doolittle, H. Ma, and M. S. Champion, "Digital Low-Level RF Control using Non-IQ Sampling," in *Proceedings of LINAC 2006, Knoxville, Tennessee USA*. Citeseer, 2006, pp. 568–570.
- [4] C. Wolf, "PicoRV32 – A Size-Optimized RISC-V CPU," <https://github.com/cliffordwolf/picorv32>, 2015.
- [5] C. Serrano and L. Doolittle, "FPGA Communications based on Gigabit Ethernet," in *13th International Conference on Accelerator and Large Experimental Physics Control Systems 2011, Grenoble, France*, 2011.